Inorganic Chemistry

Article

pubs.acs.org/IC

A Comparative Insight of Potassium Vanadates as Positive Electrode Materials for Li Batteries: Influence of the Long-Range and Local Structure

Rita Baddour-Hadjean,*[,†] Arezki Boudaoud,[†] Stéphane Bach,[†,‡] Nicolas Emery,[†] and Jean-Pierre Pereira-Ramos[†]

[†]Institut de Chimie et des Matériaux Paris Est, ICMPE/GESMAT, UMR 7182 CNRS-Université Paris Est Créteil, CNRS 2 rue Henri Dunant 94320 Thiais, France

[‡]Département Chimie, Université d'Evry Val d'Essonne, Bd F. Mitterrand, 91025 Evry, France

Supporting Information

ABSTRACT: Potassium vanadates with ratio K/V = 1:3, 1:4, and 1:8, prepared by a fast and facile synthesis route, were investigated as positive electrode materials in lithium batteries. KV_3O_8 and $K_{0.5}V_2O_5$ have layered structures, while $K_{0.25}V_2O_5$ exhibits a tunnel framework isomorphic to that of β-$Na_{0.33}V_2O_5$. The Raman spectra of KV_3O_8, $K_{0.5}V_2O_5$, and $K_{0.25}V_2O_5$ compounds are reported here for the first time, and a detailed comparative analysis distinguishes spectral patterns specific to each structural arrangement. The electrochemical performances of these potassium vanadates toward lithium insertion were investigated. The potassium-richer compound KV_3O_8 shows a good rechargeability in spite of a low discharge capacity of 70 mAh g^{-1}, while the potassium-poorer bronze $K_{0.25}V_2O_5$ exhibits the highest specific capacity of 230 mAh g^{-1} but a slow and continuous capacity fade with cycling. We demonstrate that the $K_{0.5}V_2O_5$ compound, with its double-sheet V_2O_5 layered framework characterized by a large interlayer spacing of 7.7 Å, is the best candidate as positive electrode for lithium battery among the potassium−vanadium bronzes and oxides. A remarkable specific capacity of 210 mAh g^{-1}, combined with excellent capacity retention, is achieved.

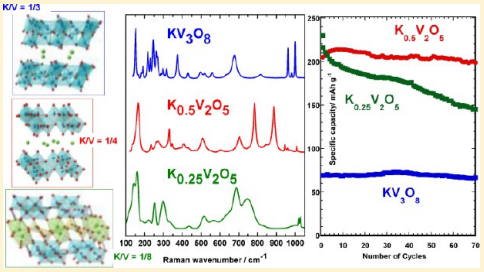

INTRODUCTION

The versatility of vanadium in terms of accessible valence states (from 3 to 5), coordination number (4−6), and coordination polyhedral shapes (tetrahedron to octahedron with intermediate square pyramid) allows a large variety of structure types to be obtained. In addition to their structural versatility, vanadium oxides and bronzes have attracted much interest owing to their interesting electrochemical activity toward lithium ions intercalation. The electrochemical behavior is known to be governed by the nature and the magnitude of the structural changes. Therefore, investigating the structural properties and the lattice dynamics of such compounds is of utmost importance to fully understand the relationships of the structure−electrochemical properties governing the electrode performances.[1]

Orthorhombic layered V_2O_5 was identified as a promising cathode material for secondary lithium batteries since the 1970s.[2,3] Its complex voltage profile with successive voltage plateaus is usually explained by the successive appearance of single-phase and large two-phase domains when discharged in the operating potential range. Recently, Raman spectroscopic studies carried out on composite[4] and thin film[5] V_2O_5 electrodes have provided detailed identification of the structural changes induced in the cathode material under operating conditions, allowing new data on the Raman spectra−structure−electrochemical properties relationships to be obtained. Sodium vanadium bronze β-$Na_{0.33}V_2O_5$, which crystallizes with the monoclinic tunnel structure, exhibits also good topotactic Li insertion/deinsertion properties[6−8], and a few optical spectroscopic studies can be found for this material.[9,10]

The idea of employing potassium vanadates as a positive electrode for lithium batteries was introduced in the 1980s by Raistrick and Huggins.[11,12] Many intercalation compounds designed by the general formula $Li_xK_yV_2O_5$ have been investigated since then.[11−14] Electrochemical lithium insertion was also reported in KV_3O_8 and $K_3V_5O_{14}$[15,16] as well as in KV_5O_{13} and $K_2V_8O_{21}$.[16] $K_2V_8O_{21}$ and KV_5O_{13} showed interesting capacities in the range of 150−200 mAh g^{-1}, with a low-capacity retention for $K_2V_8O_{21}$, while only a little Li amount reversibly entered the $K_3V_5O_{14}$ and KV_3O_8 layered compounds.[16]

In this work, a comparative study of potassium vanadates, including two vanadium bronzes and one mixed oxide as positive electrode materials for Li batteries, is reported. We show that a fast and facile solution technique leads to compounds with general formula KV_3O_8, $K_{0.5}V_2O_5$, and $K_{0.25}V_2O_5$. A detailed structural study of these materials is provided, allowing Raman fingerprints in the K−V−O system

Received: November 21, 2013
Published: January 23, 2014

dx.doi.org/10.1021/ic402897d | Inorg. Chem. 2014, 53, 1764−1772

to be newly obtained and spectral patterns specific to each structural arrangement to be revealed. Electrochemical performances are found to be strongly correlated to the structural framework of each compound. As a result, we demonstrate that the $K_{0.5}V_2O_5$ material, with double-sheet V_2O_5 framework characterized by a large interlayer spacing of 7.7 Å, is a new and promising candidate as positive electrode for rechargeable lithium batteries, the best among the potassium–vanadium bronzes and oxides, with a remarkable specific capacity of 210 mAh g^{-1} combined with excellent capacity retention.

EXPERIMENTAL SECTION

Potassium vanadates were synthesized by a solution route using 1 g of V_2O_5 (Alfa Aesar 99.995%) and stoichiometric amounts of KVO_3 or $KHCO_3$ dissolved in 10 cm^3 of an aqueous solution with 30 cm^3 H_2O_2 (30%). A fast and exothermic reaction takes place, leading to a fine precipitate. An appropriate heat treatment is then performed to obtain the potassium vanadates. V_2O_5 and KVO_3 were used as precursors for the synthesis of $K_{0.25}V_2O_5$ and $K_{0.5}V_2O_5$ vanadates at stoichiometric ratios of K/V = 1:8 and 1:4, respectively. The obtained compounds are then treated at 570 °C for 5 h under argon atmosphere. To synthesize the KV_3O_8 vanadate, we used V_2O_5 and $KHCO_3$ powders in stoichiometric ratio of K/V = 1:3. The solid compound was then treated at 500 °C for 5 h in air.

Elemental analyses combined with redox titration analysis were carried out to determine the oxidation state of vanadium ions in the potassium vanadates. This leads to the chemical compositions of $K_{0.5\pm0.02}V_2O_5$ and KV_3O_8, corresponding to potassium mixed oxides and $K_{0.25\pm0.01}V_2O_5$ for the potassium bronze.

XRD experiments were performed using a Panalytical XPert pro apparatus equipped with an X'Celerator detector and using Co Kα radiation (λ K_α = 1.789 Å). Rietveld refinements were performed with GSAS software.[17,18]

The SEM experiments were carried out using a LEO 1530 instrument.

The Raman spectra were obtained with a LaBRAM HR 800 (Jobin–Yvon–Horiba) Raman microspectrometer that included Edge filters and was equipped for signal detection with a back-illuminated charge-coupled device detector (Spex CCD) cooled by Peltier effect to 200 K. A He–Ne laser (632.8 nm) was used as the excitation source. The spectra were measured in backscattering geometry. The resolution was about 0.5 cm^{-1}. A 100× objective was used to focus the laser light on sample surface to a spot size of 1 μm^2. To avoid local heating of the sample, the power of the laser beam was adjusted to 0.2–0.5 mW with neutral filters of various optical densities.

The electrochemical experiments were performed in a stainless-steel 2025 coin-type cell (20 mm outside diameter and 2.5 mm thickness). The positive electrode was made of the active material (80 wt %), acetylene black (7.5 wt %), graphite (7.5 wt %), and Teflon as binder agent (5 wt %). The mixture was pressed on a stainless-steel grid under a pressure of 5 tons per cm^2. Li sheet was used as negative electrode. The separator was a microporous polypropylene Cellgard sheet. The cell was filled with a commercial-grade LP71 electrolyte (Merck) that means 1 M $LiPF_6$ ethylene carbonate (EC)/ diethyl carbonate (DEC)/ dimethyl carbonate (DMC) = 1:1:1). Galvanostatic experiments were made with a VMP3 Biologic apparatus.

RESULTS AND DISCUSSION

1. Structural Characterization. The obtained powders were characterized with X-ray diffraction and SEM to check the phase purity and the crystal structure as well as the particle morphology and size.

SEM images (Figure 1) reveal well-defined and regular platelets about 10 μm long, 1 μm wide, and 0.5 μm thick for the $K_{0.5}V_2O_5$ and $K_{0.25}V_2O_5$ powders, while packs of 2–10 μm stacked plates are observed for the KV_3O_8 compound.

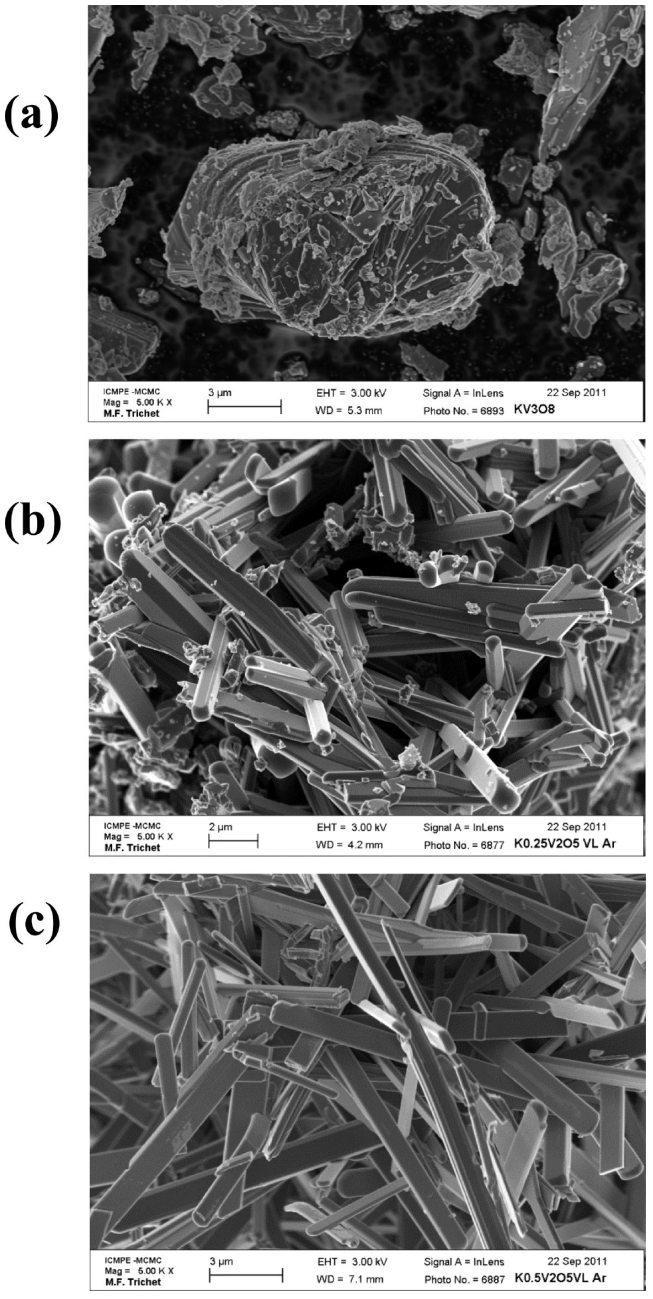

Figure 1. SEM micrographs of the (a) KV_3O_8, (b) $K_{0.25}V_2O_5$, and (c) $K_{0.5}V_2O_5$ powders.

XRD patterns of the powders are shown in Figure 2. All diffraction peaks are indexed to monoclinic KV_3O_8, $K_{0.25}V_2O_5$, and $K_{0.5}V_2O_5$ crystal phases, respectively, with the lattice parameters reported in Table 1. No peaks from other phases are detected, indicating that samples are pure. Rietveld refinement details for KV_3O_8 and $K_{0.25}V_2O_5$ are given in the Supporting Information, S1 and S2. Atomic parameters and isotropic temperature factors of $K_{0.5}V_2O_5$ retrieved from reference 19 are listed in Supporting Information, S3. V–O bond distances in the potassium vanadates are listed in Tables 2 and 3, with those of V_2O_5 reported for comparison.

The KV_3O_8 mixed oxide crystallizes in the monoclinic symmetry ($P2_1/m$, Z = 2) and involves a three-dimensional structure isomorphic to that previously reported for CsV_3O_8.[20,21] The unit cell parameters (Table 1) are in good

dx.doi.org/10.1021/ic402897d | Inorg. Chem. 2014, 53, 1764–1772

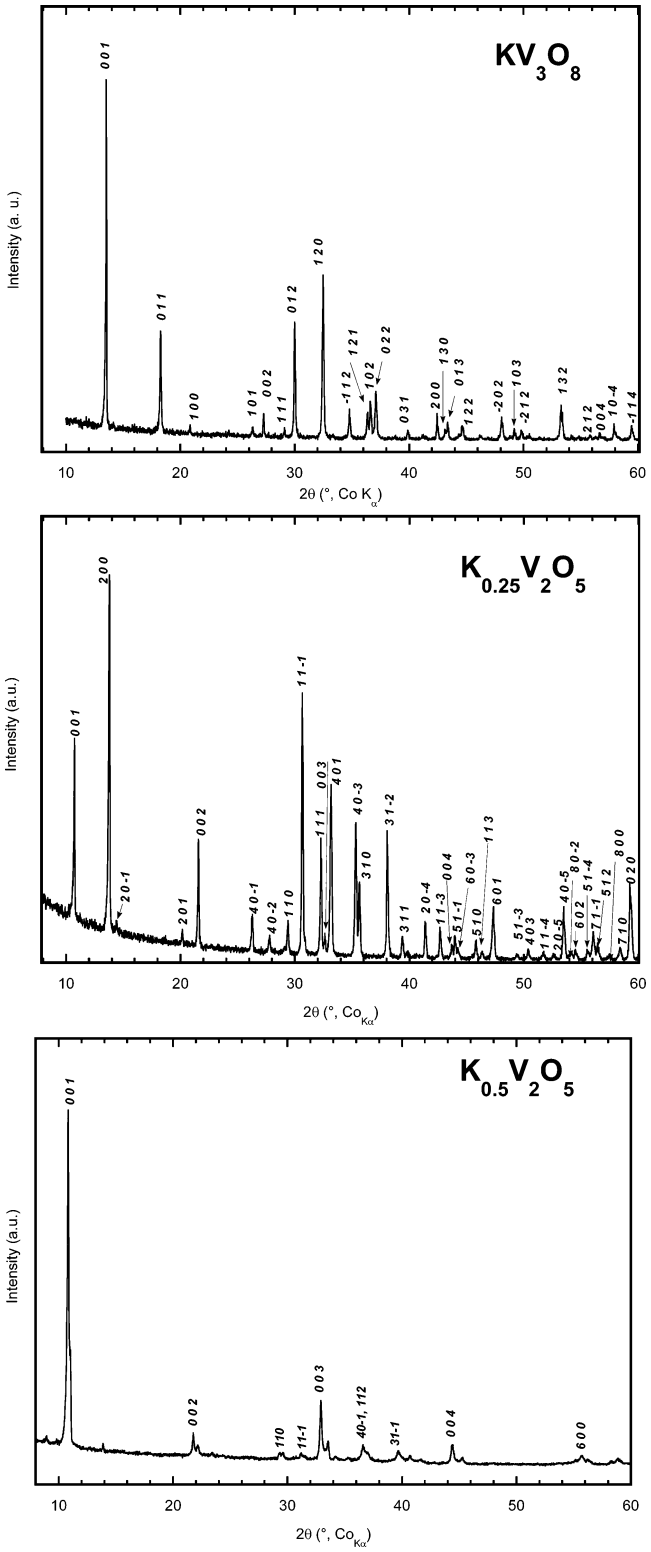

Figure 2. X-ray diffraction patterns of the (top) KV_3O_8, (middle) $K_{0.25}V_2O_5$, and (bottom) $K_{0.5}V_2O_5$ powders.

accordance with previous data. As depicted in Figure 3, KV_3O_8 adopts a layered structure with corrugated V_3O_8 layers consisting of $(V1)O_6$ octahedra and $(V2)_2O_8$ units of edge-sharing $(V2)O_5$–$(V2)O_5$ square pyramids stacking along the *c* axis. These VO_6 octahedron and VO_5 square-based pyramids are highly distorted, as reflected by the very different bond distances observed, ranging from 1.56 to 2.31 Å (Table 2).

Table 1. Unit Cell Parameters for the KV_3O_8, $K_{0.25}V_2O_5$, and $K_{0.5}V_2O_5$ Compounds

compound	space group	*a* (Å)	*b* (Å)	*c* (Å)	*β* (deg)
KV_3O_8	$P2_1/m$	4.98	8.38	7.64	96.97
$K_{0.25}V_2O_5$	$C2/m$	15.75	3.617	10.12	109.28
$K_{0.5}V_2O_5$	$C2/m$	11.68	3.67	9.5	92.24

Table 2. V–O Bond Distances (Å) in KV_3O_8, $K_{0.5}V_2O_5$,[19] and V_2O_5[27]

KV_3O_8 (this Work)		
$(V1)O_6$	$V_1–O_1$	2.308(13)
	$V_1–O_2$	1.560(15)
	$V_1–O_3$	1.866(10)
	$V_1–O_3$	1.866(10)
	$V_1–O_4$	2.022(9)
	$V_1–O_4$	2.022(9)
$(V2)O_5$	$V_2–O_1$	1.839(7)
	$V_2–O_3$	2.014(10)
	$V_2–O_3$	1.939(8)
	$V_2–O_4$	1.665(9)
	$V_2–O_5$	1.567(8)
$K_{0.5}V_2O_5$[19]		
$(V1)O_6$	$V_1–O_1$	1.899(2)
	$V_1–O_1$	1.899(2)
	$V_1–O_2$	2.376(8)
	$V_1–O_2$	1.793(7)
	$V_1–O_3$	2.082(7)
	$V_1–O_4$	1.607(7)
$(V2)O_6$	$V_2–O_1$	1.980(7)
	$V_2–O_2$	1.867(7)
	$V_2–O_3$	1.912(2)
	$V_2–O_3$	1.912(2)
	$V_2–O_3$	2.516(7)
	$V_2–O_5$	1.600(8)
V_2O_5[27]		
VO_6	$V–O_1$	1.577
	$V–O_2$	1.878
	$V–O_2$	1.878
	$V–O_3$	1.779
	$V–O_4$	2.017
	$V–O_4$	2.791

Interlayer K atoms are sandwiched just by VO_6 octahedral faces.

The $K_{0.25}V_2O_5$ bronze crystallizes in the $C2/m$ space group (Z = 6) [JCPDS file 39–0889], with unit cell parameters reported in Table 1. Its structural framework is isomorphic to the well-known Wadsley β-$Na_{0.33}V_2O_5$ phase.[22,23] Indeed, large cations such as K^+ stabilize the structure for lower alkali contents.[24] The $K_{0.25}V_2O_5$ monoclinic crystal structure is typical of all β-vanadium bronzes and contains tunnels formed by the association of VO_6 and VO_5 frameworks along the *b* axis, with V–O bond distances ranging from 1.58 to 2.37 Å (Table 3). This leads to zigzag double chains composed of edge-sharing $(V1)O_6$ and corner-sharing $(V2)O_6$ distorted octahedra as well as edge-sharing $(V3)O_5$ square-based pyramids (Figure 4). The enclosed tunnel along the *b* axis is occupied by guest cation K^+.

The XRD pattern due to $K_{0.5}V_2O_5$ bronze compares very well with the literature reports [JCPDS file 39–0890] of samples with the same composition obtained from hydrothermal[19] and microwave[25] synthesis. In our experiments, *00l*

dx.doi.org/10.1021/ic402897d | Inorg. Chem. 2014, 53, 1764–1772

Table 3. V−O Bond Distances (Å) for $K_{0.25}V_2O_5$

$(V1)O_6$	V_1-O_4	1.585(9)
	V_1-O_2	1.8597(24)
	V_1-O_2	1.8597(24)
	V_1-O_5	1.926(12)
	V_1-O_3	1.997(9)
	V_1-O_2	2.374(8)
$(V2)O_6$	V_2-O_6	1.608(9)
	V_2-O_1	1.7797(31)
	V_2-O_3	1.8961(29)
	V_2-O_3	1.8961(29)
	V_2-O_5	2.256(11)
	V_2-O_2	2.365(9)
$(V3)O_5$	V_3-O_8	1.610(8)
	V_3-O_5	1.795(11)
	V_3-O_7	1.8599(25)
	V_3-O_7	1.8599(25)
	V_3-O_7	1.984(8)
	V_3-O_6	2.58051(4)

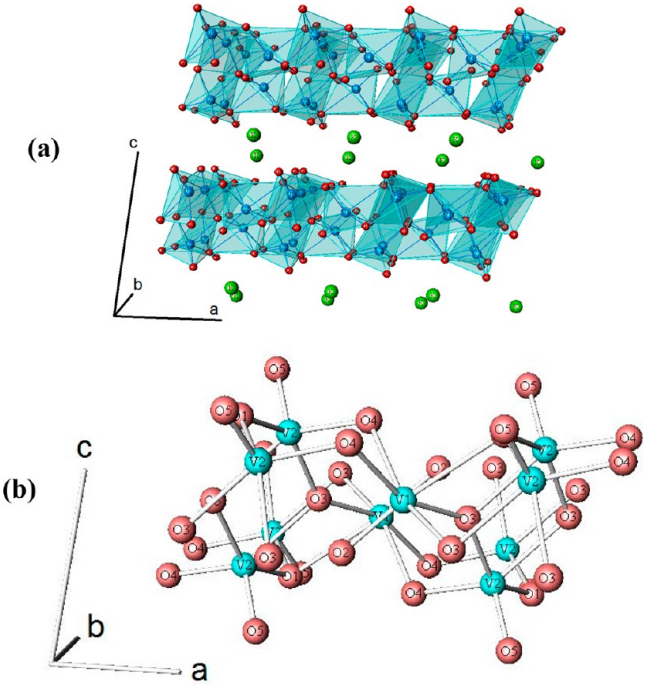

Figure 3. (a) Structure of KV_3O_8. (b) Schematic V−O polyhedra structure of the V_3O_8 layers.

lines exhibit high relative intensities, which suggest a high preferred orientation, as previously observed on microwave-synthesized powders.[25] However, in the latter case larger particles with many defects and a heterogeneous size distribution were obtained. In good accordance with previous single-crystal XRD analysis,[19] the present $K_{0.5}V_2O_5$ compound adopts the monoclinic structure $C2/m$ ($Z = 4$) isomorphic to that of $Na_{0.56}V_2O_5$ and δ-$Ag_{0.68}V_2O_5$, with $a = 11.68$ Å, $b = 3.67$ Å, $c = 9.50$ Å, and $\beta = 92.24°$.[24,26] Figure 5 clearly shows that the $K_{0.5}V_2O_5$ structure consists of double-sheet V_2O_5 layers built of $(V1)O_6$ and $(V2)O_6$ octahedra and interstitial K atoms, with V−O bond distances ranging from 1.60 to 2.52 Å (Table 2).

2. Vibrational Spectroscopy Study. The KV_3O_8, $K_{0.25}V_2O_5$, and $K_{0.5}V_2O_5$ vanadates all belong to the C_{2h} point

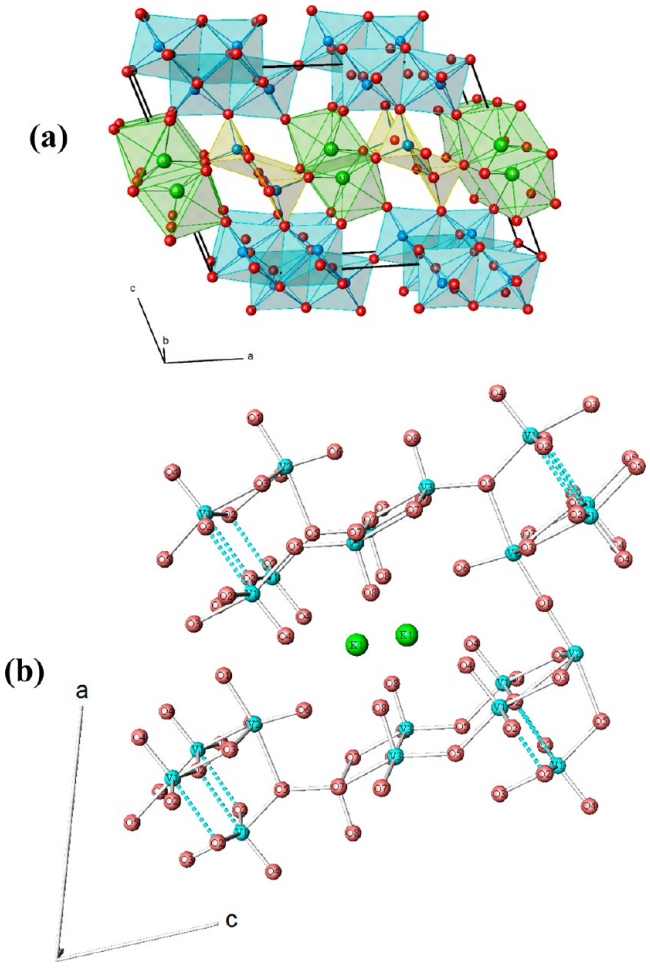

Figure 4. (a) Structure of $K_{0.25}V_2O_5$. (b) Schematic V−O polyhedra structure.

symmetry group. Factor group analysis yields the allowed representations for each one of the selected Wyckoff positions (Supporting Information, Table S4). Summarizing the overall contribution and subtracting the acoustic modes ($\Gamma_{ac} = A_u + 2B_u$), we obtain the following irreducible representations of the KV_3O_8, $K_{0.25}V_2O_5$, and $K_{0.5}V_2O_5$ vibrational modes:

$$\Gamma(KV_3O_8) = 20A_g + 16B_g + 15A_u + 18B_{2u}$$

$$\Gamma(K_{0.25}V_2O_5) = 22A_g + 11B_g + 11A_u + 22B_{2u}$$

$$\Gamma(K_{0.5}V_2O_5) = 16A_g + 8B_g + 7A_u + 14B_{2u}$$

Thus 36 Raman active modes are expected to show up in the Raman spectrum of KV_3O_8, 33 modes for $K_{0.25}V_2O_5$, and 24 modes for $K_{0.5}V_2O_5$. In this study, as in many spectroscopic studies of solids, the number of modes experimentally observed is significantly lower than that predicted by group theory methods. This situation occurs because of small polarizability derivatives for many Raman active modes, and small frequency shift separation components, for example, B_g modes, almost coincide with A_g modes.

The Raman spectra of the potassium vanadates are shown in Figure 6, with their band decomposition shown below. The spectral profiles show clearly 19, 17, and 21 Raman modes in the 95−1050 cm^{-1} wavenumber region for KV_3O_8, $K_{0.25}V_2O_5$, and $K_{0.5}V_2O_5$, respectively. Most of them correspond to the

dx.doi.org/10.1021/ic402897d | Inorg. Chem. 2014, 53, 1764−1772

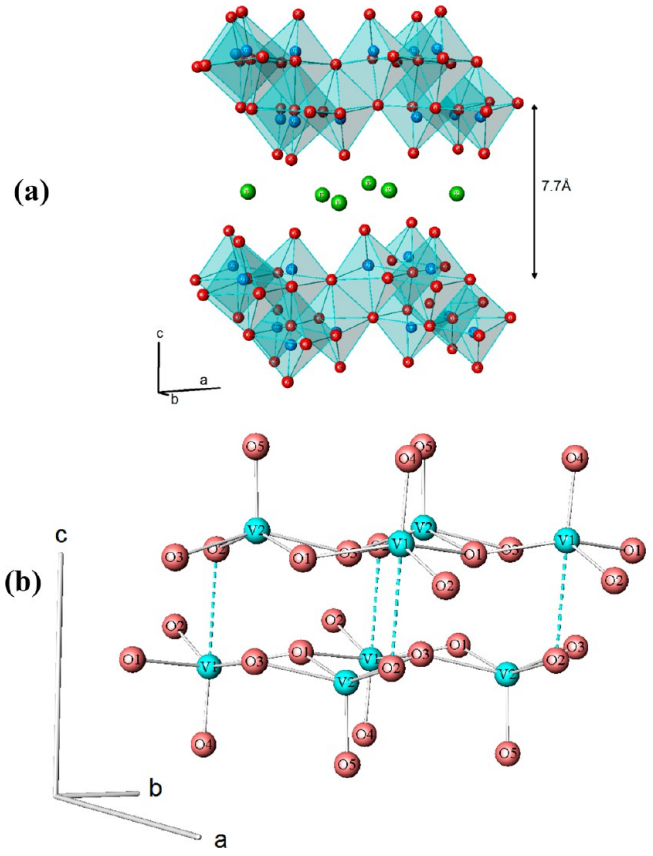

Figure 5. (a) Structure of $K_{0.5}V_2O_5$, from reference 19. (b) Schematic V−O polyhedra structure of the double layers.

stretching and bending vibrations of the different V−O and V−O−V bonds, which can be more easily viewed in Figures 3b, 4b, and 5b, respectively. Although it is difficult to unambiguously determine symmetry-based assignments from our Raman experiments, several vibrational bands can be assigned with some degree of confidence from a comparative analysis of the present Raman features with those previously reported for layered orthorhombic V_2O_5[27] and tunnel β-$Na_{0.33}V_2O_5$ bronze.[10]

The interpretation of the Raman spectra of KV_3O_8 and $K_{0.5}V_2O_5$ is made by comparison with the spectrum of V_2O_5 (Table 4). Indeed, in the same manner as V_2O_5, many of the internal optic modes wavenumbers of the KV_3O_8 and $K_{0.5}V_2O_5$ crystals are determined by the vanadium−oxygen bonds in the layers. Nevertheless, as the layer organization differs from one compound to another, VO_6/VO_5 units being linked to form either $[V_3O_8]_n$ or $[V_2O_5]_n$ arrays, some discrepancies are expected to be revealed in their Raman spectra. Raman bands in the low-frequency region (below 200 cm^{-1}) are associated with the modes involving displacements of the V atoms.

The Raman spectrum of KV_3O_8 (Figure 6 and Table 4) exhibits 19 modes located at 152, 190, 217, 231, 246, 264, 296, 317, 375, 430, 497, 520, 559, 638, 677, 816, 962, 981, and 1000 cm^{-1}. The two high-frequency bands at 962 and 1000 cm^{-1} can be assigned to the stretching ν(V=O) vibrations of the short terminal V1−O2 and V2−O5 bonds (Table 2, Figure 3b). Their high relative intensities suggest that they probably belong to the A_g symmetry species. The 1000 cm^{-1} band corresponds probably to the V2−O5 stretching vibration of the VO_5 pyramids, and the 962 cm^{-1} band corresponds to the V1−O2

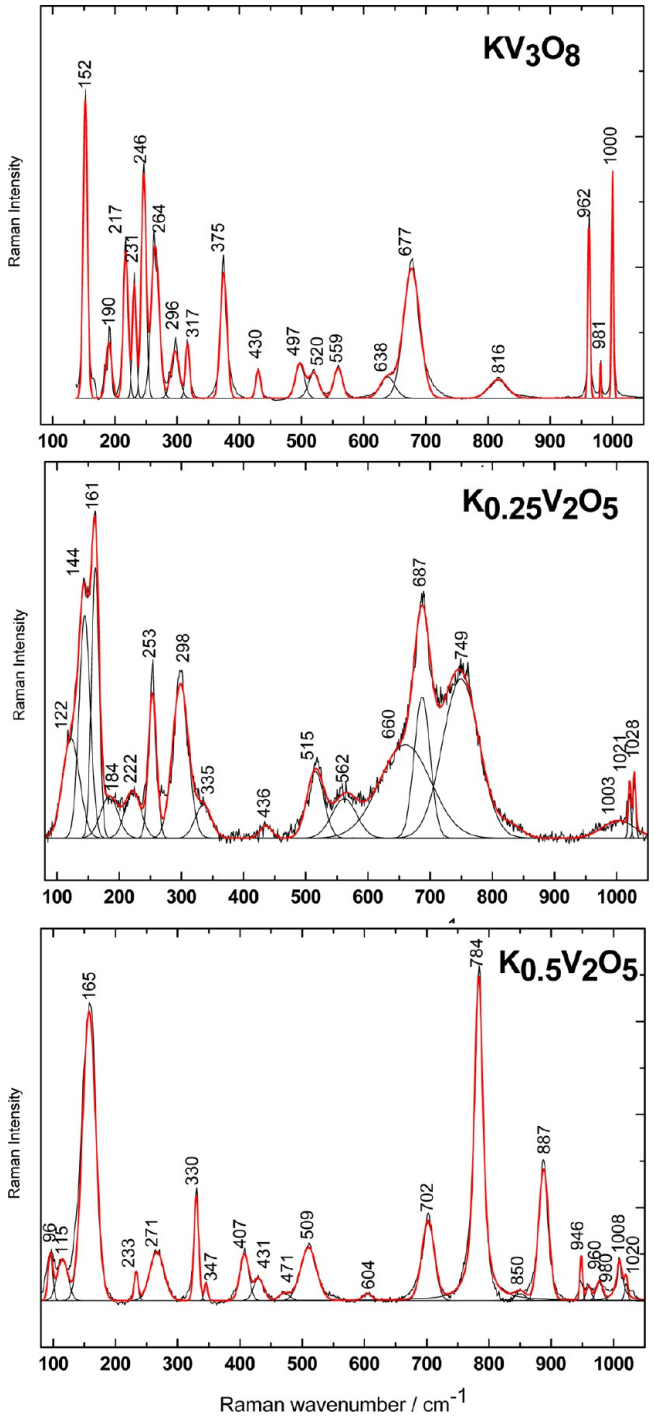

Figure 6. Raman spectra (in red color) of the (top) KV_3O_8, (middle) $K_{0.25}V_2O_5$, and (bottom) $K_{0.5}V_2O_5$ powders. Band decompositions are shown below in black color.

stretching vibration of the VO_6 octahedron. The low-intensity band at 981 cm^{-1} may be correlated with the weak feature belonging to the B_{2g} symmetry species observed at 976 cm^{-1} in the spectrum of V_2O_5.[28] The 848 cm^{-1} mode, of B_{2g} symmetry, was not detected experimentally for V_2O_5 because of its low intensity due to the antisymmetric stretching character of the V−O bonds vibration in nearly linear V−O−V bridge that leads to compensation effect.[27] This mode would correspond to the Raman band observed at 816 cm^{-1} for KV_3O_8. It may be attributed to the antiphase stretching of the V2−O4 bonds

dx.doi.org/10.1021/ic402897d | Inorg. Chem. 2014, 53, 1764−1772

Table 4. Raman Wavenumbers (cm^{-1}) and Assignments of KV_3O_8 and $K_{0.5}V_2O_5$, with Those of V_2O_5[27] Reported for Comparison

Vibrational modes		V_2O_5 [27]	KV_3O_8 [this work]		$K_{0.5}V_2O_5$ [this work]	
A_g		104			96, 115	X,Y,Z(V)
B_{1g}, B_{3g}		144	152	X,Y,Z(V)	165	
A_g, B_{2g}		195	190			
B_{3g}		220[a]	217		233	
			231			
			246			
			264	δ(V-O-V)		
B_{1g}, B_{3g}		282	296		271	δ(V-O-V)
A_g		302				
B_{2g}		310[a]	317		330	
B_{2g}		350[a]	375		347	
A_g		403	430		407	
					431	
A_g	ν(V-O3-V)	480			471	
B_{2g}	ν(V-O4)	502[a]	497		509	
A_g	ν(V-O4)	526	520			
			559		604	
				ν(V-O)		ν(V-O)
			638			
B_{1g}, B_{3g}	ν(V-O2)	700	677		702	
					784	ν(V1-O1-V2)
B_{2g}	ν(V-O3-V)	848[a]	816	ν(V2-O4-V1)	850	
					887	ν(V1-O3-V2)
					946	
			962	ν(V1-O2)	960	ν(V1-O4)
B_{2g}	ν(V-O1)	976[a]	981	ν(V2-O5)	980	ν(V2-O5)
A_g	ν(V-O1)	994	1000	ν(V2-O5)	1008	
					1020	

[a]Not observed experimentally.

forming the asymmetric V2−O4−V1 bridges (Figure 3b and Table 4).

Bands at lower wavenumbers observed at 497, 520, 559, 638, and 677 cm^{-1} may be assigned to the stretching vibrations of the longer V1−O3, V1−O4, V2−O1, and V2−O3 bonds. The bending δ(V−O−V) modes cover the 200−450 cm^{-1} wavenumber region. It is more difficult to determine precisely the frequency distribution for these modes because of considerable coupling.

The Raman spectrum of $K_{0.5}V_2O_5$ exhibits 21 modes located at 96, 115, 165, 233, 271, 330, 347, 407, 431, 471, 509, 604, 702, 784, 850, 887, 946, 960, 980, 1008, and 1020 cm^{-1} (Figure 6 and Table 4). In the 200−900 cm^{-1} frequency region, most of the bands have their counterpart in the Raman spectrum of the V_2O_5 crystal and may be assigned to the δ(V−O−V) bending and ν(V−O) stretching vibrations in the $(V1)O_6$ and $(V2)O_6$ octahedra.[27] In the 900−1020 cm^{-1} range, the stretching vibrations of the shortest V═O bonds of 1.6 Å (V1−O4 and V2−O5) are observed (Table 2, Figure 5b). Multiple features (at 946, 960, 980, 1008, and 1020 cm^{-1}) are clearly highlighted in this region for $K_{0.5}V_2O_5$, compared to two bands at 994 cm^{-1} and 976 cm^{-1} in V_2O_5. This multiplicity may be due to the presence of two short bonds in $K_{0.5}V_2O_5$ instead of a single one in V_2O_5, combined with the existence of both V^{4+}═O and V^{5+}═O species in the bronze. Also worth noting are the intense Raman features at 784 and 887 cm^{-1}, which correspond to the stretching vibrations of strongly asymmetric V1−O1−V2

dx.doi.org/10.1021/ic402897d | Inorg. Chem. 2014, 53, 1764−1772

and V1−O3−V2 bridges in the double-layer structure of $K_{0.5}V_2O_5$ (Figure 5b).

The Raman spectrum of $K_{0.25}V_2O_5$ (Figure 6 and Table 5) exhibits 17 modes located at 122, 144, 161, 184, 222, 253, 298, 335, 436, 515, 562, 660, 687, 749, 1003, 1021, and 1028 cm^{-1}. These features coincide very well with those observed for the isomorphic β-$Na_{0.33}V_2O_5$ bronze, which are listed in Table 5 for comparison.[10] Hence, phonon modes below 400 cm^{-1} originate from the bond bending vibrations, while the higher-frequency modes are due to the stretching vibrations of the different V−O bonds in the $(V1)O_6$, $(V2)O_6$, and $(V3)O_5$ polyhedra (see Table 3 and Figure 4b). Thirteen A_g symmetry modes can be assigned at 122, 144, 222, 253, 298, 335, 436, 515, 562, 749, 1003, 1021, and 1028 cm^{-1}, whereas four B_g symmetry modes may correspond to the Raman lines observed at 161, 184, 660, and 687 cm^{-1}. The highest-frequency modes are assigned to the stretching vibrations of the shortest V−O bonds in the $(V1)O_6$, $(V2)O_6$, and $(V3)O_5$ polyhedra. The Raman band at 1028 cm^{-1} represents the V3−O8 stretching vibration, the mode at 1021 cm^{-1} originates from the V2−O6 bond, and the 1003 cm^{-1} comes from the V1−O4 bond stretching vibrations. The 749 cm^{-1} mode is assigned to the V3−O5 and V1−O5 oscillations. The 687 cm^{-1} mode corresponds to the antisymmetric V1−O2−V1 stretching mode. The B_g symmetry mode at 660 cm^{-1} can be assigned both to the V3−O7 (along *b* axis) and to the V2−O3 stretching mode. The A_g symmetry modes observed at 562 cm^{-1} and 515 cm^{-1} correspond to the V1−O3 and V3−O7 (along *c* axis) stretching vibrations, respectively. Potential energy distribution calculations are in progress to complete this preliminary spectroscopic analysis.

Table 5. Raman Wavenumbers (cm^{-1}) of $K_{0.25}V_2O_5$ Raman Wavenumbers and Band Assignments of $Na_{0.33}V_2O_5$[10] Are Also Reported for Comparison

symmetry species	β-$Na_{0.33}V_2O_5$[10]	assignment	β-$K_{0.25}V_2O_5$ [this Work]
A_g	1027	$\nu(V_3-O_8)$	1028
	1013	$\nu(V_2-O_6)$	1021
	990	$\nu(V_1-O_4)$	1003
	747	$\nu(V_3-O_5) + \nu(V_1-O_5)$	749
	556	$\nu(V_1-O_3)$	562
	516	$\nu(V_3-O_7)$ //*c*	515
	462		
	440		436
	390		
	333		335
	288		298
	256		253
	223		222
	124		144
			122
B_g	697	$\nu_{as}(V_1-O_2-V_1)$	687
	657	$\nu(V_2-O_3) + \nu(V_3-O_7)$ //*b*	660
	275		
			184
	151		161

3. Electrochemical Study. The first discharge−charge cycle of the potassium vanadates at C/10 in the 4−2 V potential range are shown in Figure 7. Clearly, the electrochemical fingerprints of the KV_3O_8, $K_{0.25}V_2O_5$, and $K_{0.5}V_2O_5$ vanadates strongly differ from one to another according to the different crystalline structures of the vanadates. Sharp discontinuities are observed in the discharge−charge profile of the $K_{0.25}V_2O_5$ tunnel structure (Figure 7a), whereas the KV_3O_8 and $K_{0.5}V_2O_5$ electrode materials both exhibit a common discharge−charge profile characterized by a smooth decline of the working potential versus Li content (Figure 7b,c), which is specific to layered-type compounds.

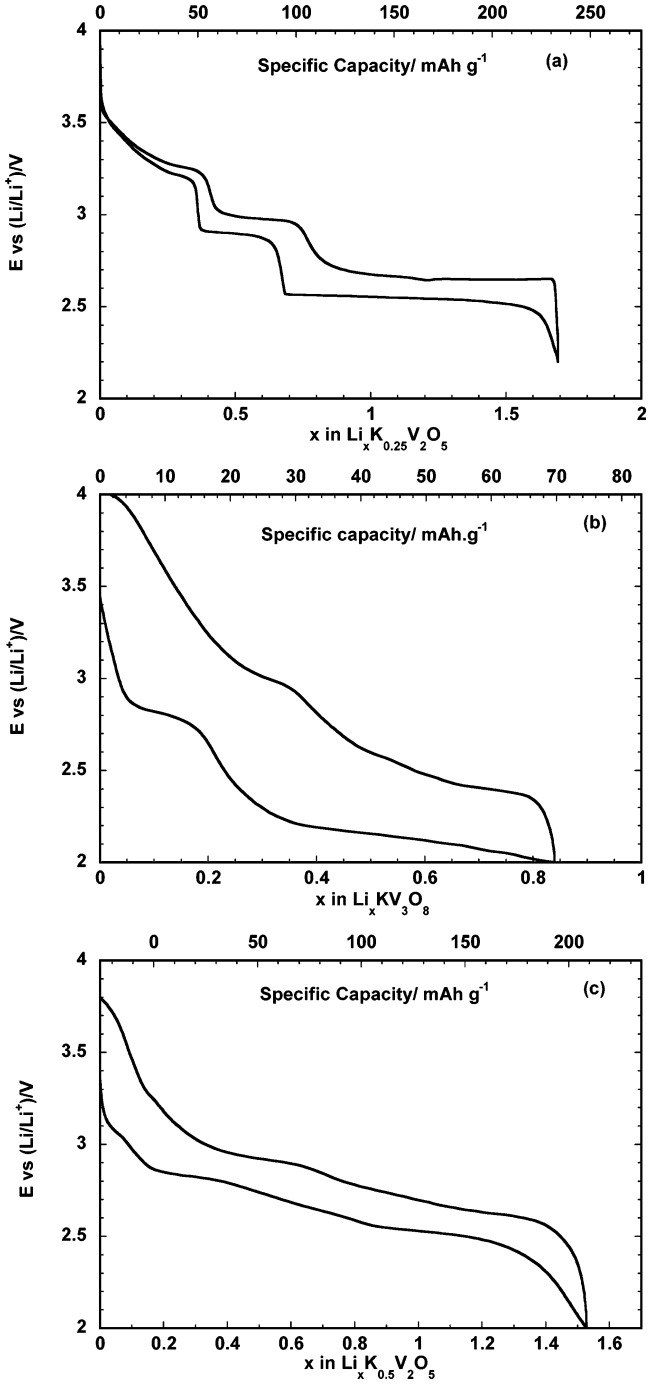

Figure 7. Typical galvanostatic discharge−charge curves obtained at C/10 rate for the (a) $K_{0.25}V_2O_5$, (b) KV_3O_8, and (c) $K_{0.5}V_2O_5$ composite electrodes.

Electrochemical lithium insertion into $K_{0.25}V_2O_5$ involves three main steps in the potential window of 3.6/2.2 V. These different steps are well-separated by two sudden potential drops for x = 0.38 and x = 0.68. The working voltage continuously

dx.doi.org/10.1021/ic402897d | Inorg. Chem. 2014, 53, 1764−1772

decreases from 3.6 to 3.2 V for $0 < x < 0.4$. The second and the third steps consist in two voltage plateaus at 2.9 and 2.55 V for lithium contents, corresponding to $0.38 \leq x \leq 0.68$ and $0.68 \leq x \leq 1.7$, respectively. The overall related specific capacity is high since it reaches 230 mAh g^{-1}. These electrochemical features correspond to a filling scheme of specific crystallographic sites in the $K_{0.25}V_2O_5$ bronze.[10,11,13] Indeed, it has been shown that Li accommodation in tunnel $M_xV_2O_5$ bronzes occurs in particular sites with strong repulsive Coulombic interactions.[6,7] Note that the whole inserted lithium ions can be removed from the tunnel structure of the β-$K_{0.25}V_2O_5$ bronze, as shown by the quantitative charge process (Figure 7a).

Figure 7b,c shows a substantial difference in the electrochemical fingerprint of $K_{0.5}V_2O_5$, when compared with KV_3O_8. Indeed, whereas the KV_3O_8 mixed oxide is characterized by a very low capacity of ~70 mAh g^{-1} (Figure 7b), in good accordance with previous studies,[15,16] a 3 times higher specific capacity of 210 mAh g^{-1} is achieved for the $K_{0.5}V_2O_5$ compound (Figure 7c). Figure 7b,c shows also that KV_3O_8 mixed oxide exhibits a higher hysteresis between discharge and charge, when compared to $K_{0.5}V_2O_5$ (750 mV against 200 mV). These observations suggest that the electron transfer is more difficult in the corrugated (*ab*) sheets of the KV_3O_8 oxide than it is in the planar double-layered $K_{0.5}V_2O_5$ bronze.

The discharge curve of $K_{0.5}V_2O_5$ shows three insertion steps located at 3 V, 2.8 V, and 2.5 V, with corresponding Li uptakes of ~0.2, 0.6, and 0.7 Li per mole of bronze, respectively. The total faradaic yield of 1.5 F/mol involved in the reduction process exactly corresponds to the number of available V^{5+} ions in $K_{0.5}V_2O_5$. Worth noting is the highly reversible behavior evidenced during Li extraction up to 3.75 V, leading to the Li-free host structure. The layered structure of $K_{0.5}V_2O_5$ characterized by a large interlayer spacing of 7.7 Å (Figure 5a), about twice that encountered in the V_2O_5 parent oxide (4.37 Å), probably explains a facile and reversible Li insertion−extraction process.

Cycling experiments have been carried out at C/10 rate in the 4−2 V potential range. Figure 8 shows the evolution of the specific capacity as a function of the cycle number for the three potassium vanadates. In spite of the best initial discharge capacity with 230 mAh g^{-1}, the tunnel compound $K_{0.25}V_2O_5$ shows a progressive and continuous decline of the discharge capacity, with only 66% of the initial capacity (e.g., 153 mAh g^{-1}) recovered after 70 cycles. Conversely, the lowest initial discharge capacity of 70 mAh g^{-1} achieved for KV_3O_8 is retained over all of the 70 cycles. The most remarkable behavior is observed for the layered structure of $K_{0.5}V_2O_5$, which exhibits excellent capacity retention since 200 mAh g^{-1} are still recovered after 70 cycles. Further electrochemical and structural studies of $K_{0.5}V_2O_5$ as rechargeable cathode material confirm these promising data and will be reported elsewhere.[29]

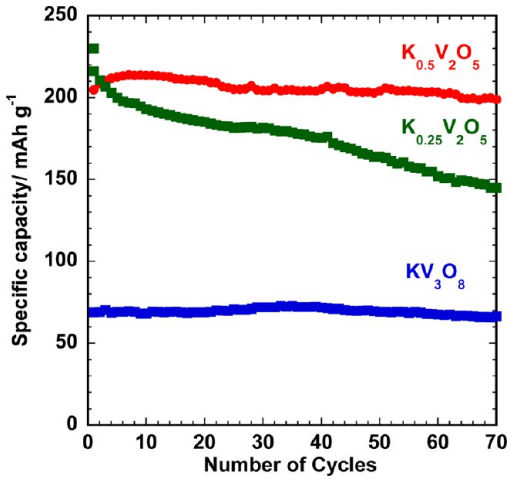

Figure 8. Evolution of the discharge capacity vs the number of cycles recovered at C/10 rate for the (blue) KV_3O_8, (green) $K_{0.25}V_2O_5$, and (red) $K_{0.5}V_2O_5$ composite electrodes in the 4−2 V potential range.

CONCLUSION

Potassium vanadates with ratio K/V = 1:3, 1:4, and 1:8 have been synthesized through a fast and facile solution route, and their structural and electrochemical behaviors toward Li insertion are reported. While KV_3O_8 and $K_{0.5}V_2O_5$ compounds involve three-dimensional structures made of V_3O_8 layers and double-sheet V_2O_5 layers, respectively, the $K_{0.25}V_2O_5$ bronze exhibits a tunnel structure isomorphic to that of β-$Na_{0.33}V_2O_5$. The Raman spectra of these compounds are reported here for the first time. By making a comparative analysis of the vibrational states of KV_3O_8, $K_{0.5}V_2O_5$, and V_2O_5 on one hand and $K_{0.25}V_2O_5$ and β-$Na_{0.33}V_2O_5$ on the other, spectral patterns specific to each structural arrangement are found, and a preliminary assignment scheme for each compound is proposed. In particular, intense Raman features in the 750−900 cm^{-1} region have been ascribed to the existence of intralayer highly asymmetric V−O−V bridges in the $K_{0.5}V_2O_5$ bronze. Furthermore, among these potassium vanadates, $K_{0.5}V_2O_5$ is shown to be a new and promising cathode for rechargeable Li batteries. Operating at an average voltage of 2.6 V, it delivers a reversible capacity of 210 mAh g^{-1} and excellent cycle life (200 mAh g^{-1} at C/10 after 70 cycles). This finding is probably related to the unusual large interlayer spacing of 7.7 Å combined with K^+ ions, which stabilize the stacking of double-sheet V_2O_5 layers and ensure a reversible Li accommodation−extraction process.

ASSOCIATED CONTENT

Supporting Information

Wyckoff positions and fractional atomic parameters for KV_3O_8, $K_{0.25}V_2O_5$, and $K_{0.5}V_2O_5$ and allowed representation for each atom in KV_3O_8, $K_{0.25}V_2O_5$, and $K_{0.5}V_2O_5$. This material is available free of charge via the Internet at http://pubs.acs.org.

AUTHOR INFORMATION

Corresponding Author

*E-mail: baddour@icmpe.cnrs.fr.

Notes

The authors declare no competing financial interest.

ACKNOWLEDGMENTS

This work was supported by the LIBASTRAM CNRS Project No. 6094 in the frame of international colloboration PICS program between the Centre National de la Recherche Scientifique (CNRS) and the Russian Fondation for Basic Research (RFBR).

REFERENCES

(1) Baddour-Hadjean, R.; Pereira-Ramos, J. P. *Chem. Rev.* **2010**, *110*, 1278−1319.
(2) Whittingham, M. S. *J. Electrochem. Soc.* **1975**, *122*, 526−527.

(3) Whitthingham, M. S. *Chem. Rev.* **2004**, *104*, 4271−4301.
(4) Baddour-Hadjean, R.; Marzouk, A.; Pereira-Ramos, J. P. *J. Raman Spectrosc.* **2012**, *43*, 153−160.
(5) Baddour-Hadjean, R.; Navone, C.; Pereira-Ramos, J. P. *Electrochim. Acta* **2009**, *54*, 6674−6679.
(6) Bach, S.; Pereira-Ramos, J. P.; Baffier, N.; Messina, R. *J. Electrochem. Soc.* **1990**, *137*, 1042−1048.
(7) Pereira-Ramos, J. P.; Messina, R.; Znaidi, L.; Baffier, N. *Solid State Ionics* **1988**, *28*−*30*, 886−894.
(8) Liu, H.; Wang, Y.; Li, L.; Wang, K.; Hosono, E.; Zhou, H. *J. Mater. Chem.* **2009**, *19*, 7885−7891.
(9) Franck, S.; Kuntscher, C. A.; Gregora, I.; Yamauchi, T.; Ueda, Y. *Phys. Rev. B* **2007**, *76*, 075128 (6 pages).
(10) Baddour-Hadjean, R.; Bach, S.; Emery, N.; Pereira-Ramos, J. P. *J. Mater. Chem.* **2011**, *21*, 11296−11305.
(11) Raistrick, I.; Huggins, R. *Mater. Res. Bull.* **1983**, *18*, 337−346.
(12) Raistrick, I. *Rev. Chim. Miner.* **1984**, *21*, 456−467.
(13) Pereira-Ramos, J. P.; Messina, R.; Perichon, J. *J. Electrochem. Soc.* **1988**, *135*, 3050−3057.
(14) Maingot, S.; Baffier, N.; Pereira-Ramos, J. P.; Willmann, P. *Solid State Ionics* **1993**, *67*, 29−34.
(15) West, K.; Zachau-Christiansen, B.; Jacobsen, T.; Skaarup, S. *Solid State Ionics* **1990**, *40/41*, 585−588.
(16) Manev, V.; Momchilov, A.; Nassalevska, A.; Pistoia, G.; Pasquali, M. *J. Power Sources* **1993**, *43/44*, 561−568.
(17) Larson, A. C., Von Dreele, R. B. *General Structure Analysis System (GSAS);* Technical Report LAUR86−748 for Los Alamos National Laboratory: Los Alamos, NM, 2004.
(18) Toby, B. H. *J. Appl. Crystallogr.* **2001**, *34*, 210−213.
(19) Oka, Y.; Yao, T.; Yamamoto, N. *J. Mater. Chem.* **1995**, *5*, 1423−1426.
(20) Evans, H. T.; Block, S. *Inorg. Chem.* **1966**, *5*, 1808−1814.
(21) Oka, Y.; Yao, T.; Yamamoto, N. *Mater. Res. Bull.* **1997**, *32*, 1201−1209.
(22) Wadsley, A. D. *Acta Crystallogr.* **1955**, *8*, 695−701.
(23) Galy, J.; Darriet, J.; Casalot, A.; Goodenough, J. B. *J. Solid State Chem.* **1970**, *1*, 339−348.
(24) Pouchard, M.; Hagenmuller, P. *Mater. Res. Bull.* **1967**, *2*, 799−808.
(25) Rao, K. J.; Ramankrishnan, P. A.; Gadagkar, R. *J. Solid State Chem.* **1999**, *148*, 100−107.
(26) Kanke, Y.; Kato, K.; Takayama-Muromachi, E.; Isobe, M. *Acta Crystallogr., Sect. C: Cryst. Struct. Commun.* **1990**, *46*, 536−538.
(27) Baddour-Hadjean, R.; Pereira-Ramos, J. P.; Navone, C.; Smirnov, M. *Chem. Mater.* **2008**, *20*, 1916−1923.
(28) Abello, L.; Husson, E.; Repelin, Y.; Lucazeau, G. *Spectrochim. Acta, Part A* **1983**, *39*, 641−651.
(29) Bach, S., Boudaoud, A., Emery, N., Baddour-Hadjean, R., Pereira-Ramos, J. P. *Electrochim. Acta* DOI: 10.1016/j.electacta.2013.12.039